Asymmetric ocean basins

Giuliano Panza[1], Carlo Doglioni[2], and Anatoli Levshin[3]
[1]Dipartimento di Scienze della Terra, Università di Trieste, 34127 Trieste, Italy, and Abdus Salam International Centre for Theoretical Physics (ICTP), Strada Costiera 1, 34151 Trieste, Italy
[2]Dipartimento di Scienze della Terra, Università Sapienza, 00185 Rome, Italy, and Istituto di Geologia Ambientale e Geoingegneria (Consiglio Nazionale delle Richerche, CNR-IGAG), 00185 Rome, Italy
[3]Department of Physics, University of Colorado, Boulder, Colorado 80309, USA

ABSTRACT

While the superficial expression of oceanic ridges is generally symmetric, their deeper roots may be asymmetric. Based on a surface wave tomographic three-dimensional model of the Earth's upper 300 km, we construct a global cross section parallel to the equator of the net rotation of the lithosphere, the so-called tectonic equator. Shear wave velocities indicate a difference between the western and eastern flanks of the three major oceanic rift basins (Pacific, Atlantic, and Indian ridges). In general, the western limbs have a faster velocity and thicker lithosphere relative to the eastern or northeastern one, whereas the upper asthenosphere is faster in the eastern limb than in the western limb. We interpret the difference between the two flanks as the combination of mantle depletion along the oceanic rifts and of the westward migration of the ridges and the lithosphere relative to the mantle. The low-velocity layer in the upper asthenosphere at the depth of 120–200 km is assumed to represent the decoupling between the lithosphere and the underlying mantle. It is also well defined by the distribution of radial anisotropy that reaches minimum values close to the rifts, but with an eastward offset. These results could be explained in the frame of the westward drift of the lithosphere relative to the underlying mantle.

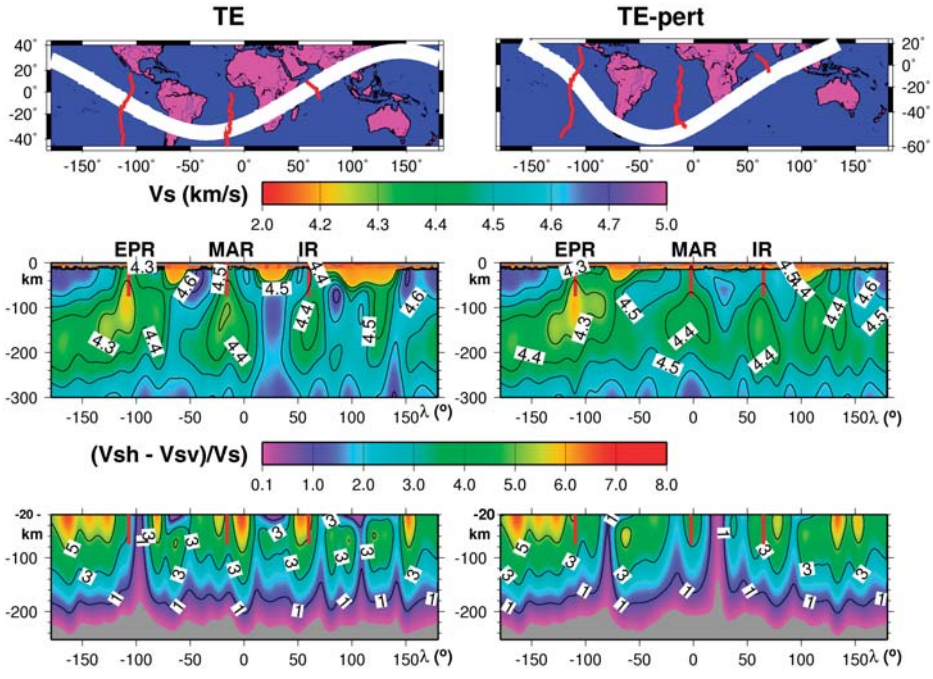

Figure 1. Shear wave (Earth's) section along tectonic equator (TE) proposed by Crespi et al. (2007) to left, and along perturbed path (TE-pert). Note generalized asymmetry across oceanic ridges: lithosphere (0–100 km) in western side of rift is faster than in eastern or northeastern side, whereas upper asthenosphere (low-velocity layer, 100–200 km) is slower in western side with respect to conjugate counterpart. Red lines correspond to elements of Eastern Pacific, Mid-Atlantic, and Indian Ridges. Lower panels show radial anisotropy along these sections. To obtain shear wave velocity (Vs) radial cross sections we used bispline interpolation of velocities at fixed depths levels (on 4 km grid) with subsequent Gaussian smoothing. Vs is taken here as average of Vsv and Vsh (see text) along section covering 10° width. Radial anisotropy sections are without crust, since crust is assumed to be isotropic.

INTRODUCTION

The mantle is thought to rise adiabatically along oceanic ridges and to melt, generating new oceanic crust (e.g., Cann et al., 1999, and references therein). Since the recognition of magnetic anomalies on both sides of the ridges, oceanic basins have generally been associated with symmetric spreading. However, it has been shown that rift zones are moving on the Earth's surface relative to the underlying mantle, i.e., they are decoupled with respect to the mantle. Plate boundaries move to the west relative to Antarctica and to the hotspot reference frame (e.g., Le Pichon, 1968; Garfunkel et al., 1986).

Many papers have described some asymmetric spreading, differences in geometry and subsidence between the two ridges, as well as heterogeneities in the underlying mantle tomography (e.g., Morgan and Smith, 1992; Zhang and Tanimoto, 1993; Calcagno and Cazenave, 1994; Cande and Kent, 1995; Bonatti et al., 2003; Pilidou et al., 2005; Müller et al., 2008).

Subduction zones show a marked asymmetry as a function of their geographic polarity (Doglioni et al., 2007); in our research we tested whether a worldwide asymmetry holds for oceanic rifts as well.

For this purpose, we extracted sections across the S-wave tomographic model of the Earth's lithosphere-asthenosphere system (Shapiro and Ritzwoller, 2002). The sections are perpendicular to the three main oceanic ridges, the East Pacific Ridge (or Rise), Mid-Atlantic Ridge, and Indian Ridge, as shown in Figure 1. The first global cross section coincides with the so-called tectonic equator, which is the ideal line along which plates move over the Earth's surface with the fastest mean angular velocity toward the west relative to the mantle (Crespi et al., 2007). The coordinates of the sections are in Table DR1 of the GSA Data Repository.[1]

[1]GSA Data Repository item 2010010, Figures DR1–DR4 (mean bathymetric cross section of the world ocean basins, showing that the eastern flank is shallower, and six Vs tomographic cross sections of other segments of the main oceanic ridges, showing the western side with faster lithosphere relative to the eastern side) and Table DR1 (geographic coordinates of the tectonic equator), is available online at www.geosociety.org/pubs/ft2010.htm, or on request from editing@geosociety.org or Documents Secretary, GSA, P.O. Box 9140, Boulder, CO 80301, USA.

THREE-DIMENSIONAL SHEAR VELOCITY MODEL

We considered a three-dimensional (3-D) shear velocity model of the Earth's upper mantle, CUB2 (Shapiro and Ritzwoller, 2002; http://ciei.colorado.edu/~nshapiro/MODEL/), obtained by tomographic inversion of seismic surface waves generated by earthquakes and recorded by numerous seismic stations across the world. It provides a quite detailed (at 2° × 2° geographical grid) shear wave velocity (Vs) image of the uppermost 300 km of the Earth. This model is the result of the Monte Carlo inversion of dispersion data-group velocities of fundamental Rayleigh and Love modes, in the range of periods 16–200 s (Levshin et al., 1989; Ritzwoller and Levshin, 1998; Ritzwoller et al., 2002), and phase velocities in the range of periods 40–200 s (Trampert and Woodhouse, 1995; Ekstrom et al., 1997). The procedure allows for the recognition of the radial anisotropy of shear velocities in the upper mantle down to 220 ± 30 km depth and provides estimates of the uncertainty in the inversion.

To obtain Vs radial cross sections across this model, we use bispline (bicubic spline) interpolation of velocities at fixed depths levels (on a 4 km grid) with subsequent Gaussian smoothing. Here the Vs is taken as an average of Vsv and Vsh along two sections (tectonic equator, TE, and along a sort of perturbed tectonic equator, TE-pert), covering 10° width (Fig. 1). The magnitude of the radial anisotropy (Vsh – Vsv)/Vs predicted by the model is shown in Figure 1.

Another section slightly deviates from the TE, along a sort of perturbed tectonic equator. Along the TE-pert, following a sort of funneling, the low-velocity zone (or low-velocity layer), corresponding to the upper asthenosphere, has a shear wave velocity lower than 4.5 km/s everywhere, i.e., all across the Earth at a depth of ~130–200 km.

The Vs model shows an asymmetry in the uppermost 100 km between the western side (4.5–4.8 km/s), which is faster with respect to the eastern side of the rift (4.4–4.6 km/s). The upper asthenosphere (100–200 km) of the western flank is slow (Vs = 4.2–4.4 km/s) compared to the eastern flank (Vs = 4.3–4.5 km/s). Therefore, the difference in Vs between the western and the eastern flanks of the rift, both in the lithosphere and in the asthenosphere, is significant and in the range of 0.1–0.3 km/s. The low-velocity layer shows an asymmetric pattern; it is deeper and thicker on the west than on the east side of the ridge. This is particularly evident in the Eastern Pacific Ridge. In the western lithosphere of the Mid-Atlantic Ridge, the Vs horizontal gradient is much larger than the one in the East Pacific Ridge, in agreement with the slower spreading rate of the Mid-Atlantic Ridge.

GEODYNAMIC MODEL

The bathymetry of rift zones is, in general, asymmetric: the eastern flank is in average slightly shallower (100–300 m) than the western flank (Doglioni et al., 2003) (see Fig. DR1). Since the mantle becomes depleted in Fe when it melts beneath a ridge (Oxburgh and Parmentier, 1977), and it moves eastward relative to the lithosphere, the shallower bathymetry to the east has been interpreted in terms of an isostatic adjustment, i.e., a lower thermal subsidence in the eastern flank of the ridge (Doglioni et al., 2005). Due to the net rotation of the lithosphere (Gripp and Gordon, 2002; Crespi et al., 2007; Husson et al., 2008), the subridge is depleted and lighter mantle will eventually transit beneath a continent to the east, if any, uplifting it (e.g., Africa; Doglioni et al., 2003).

Since rifts show a difference that appears to be chiefly controlled by the geographical distribution of the anomalies (Vs, bathymetry), we interpret the asymmetry in terms of the westward drift of the lithosphere relative to the mantle (Scoppola et al., 2006), along the TE of Crespi et al. (2007) that makes an angle of ~30° relative to the geographic equator.

The hot mantle rising along ridges is decompressed, and thus melts and delivers fluids. This process determines a chemical depletion of the pre-melting mantle: the residual mantle undergoes a modification of its physical properties, such as the decrease in density (20–60 kg/m^3; Oxburgh and Parmentier, 1977), and consequent natural increase of Vs due to Fe depletion, increase of 1–2 orders of magnitude of viscosity, and temperature decrease of ~100 °C. At shallower lithospheric depths, in the range 0–80 km, due to cooling and associated with its westward motion relative to the underlying mantle, the lithosphere is forming from depleted mantle, and has naturally lower velocities than on the western side of the ridge.

Ridges move relative to the mantle, with velocity Vr given by (Va + Vb)/2, where Va and Vb are the velocities relative to the mantle of the two plates (a and b), separated by the rift. The ridge is the site of mantle depletion due to melting, where new oceanic crust is formed (Fig. 2). The melting region of the mantle gradually shifts westward, affecting new sections of undepleted mantle. This process delivers depleted mantle to the eastern side of the rift. In other words, the residual asthenosphere shifts eastward, the upper part having cooled to form the lithospheric mantle of the eastern flank. Therefore, the ridge is permanently transiting westward over a fertile mantle able to steadily supply mid-oceanic ridge basalt melts. However, once transited, there will be a compositional depletion in the mantle that should appear when comparing the lithosphere and/or asthenosphere of the western side of the rift with its eastern conjugate counterpart. This would explain the difference in Vs observed at both sides of the rift.

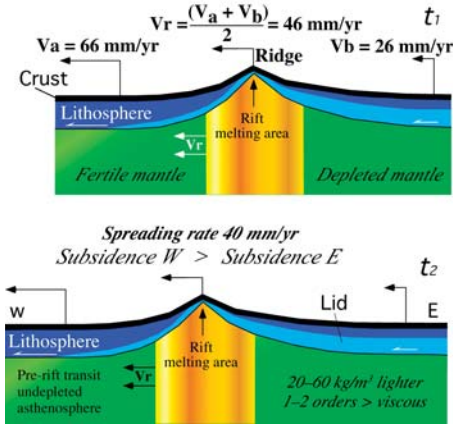

Figure 2. Oceanic rift with hypothetic velocities of plates a and b relative to fixed mantle. Ridge moves west at velocity of ridge (Vr). Separation between plates triggers uplift of undepleted mantle previously located to west. In melting area, mantle loses Fe, Mg, and other minerals to form oceanic crust, while residual mantle is depleted. Since melting area moves west it gradually transits toward undepleted mantle, releasing depleted mantle to the east. This can explain slightly shallower bathymetry of eastern limb, but it should also generate asymmetry of seismic wave velocity seen in Figure 1. In this model, differential velocity among plates is controlled by low-velocity layer viscosity variations generating variable decoupling between lithosphere and mantle (see text). t_1 and t_2 are two time stages. Lid is lithospheric mantle. Modified after Doglioni et al. (2005).

Zoomed-in images of cross sections along the TE at rift zones (East Pacific Ridge, Mid-Atlantic Ridge, Indian Ridge) show this asymmetry (Fig. 3). In order to test whether this observation is a local occasional asymmetry, a number of sections perpendicular and parallel to the ridge have been constructed along the TE (Fig. 3) and far away from it (Figs. DR2, DR3, and DR4). They are still supportive of an asymmetric pattern in the upper mantle when comparing the western and the eastern sides of the rift, particularly in the Pacific and Indian ridges.

Similarly, a slower asthenosphere in the western side of the East Pacific Ridge has been identified in the MELTS experiment, interpreted as due to more pronounced melting in the western asthenospheric mantle (e.g., Scheirer et al., 1998). There are areas where this asymmetry is not evident, or possibly sections where it is even reverse. However, it appears to be a dominant feature.

The partial melting in the mantle beneath ridges varies as a function of a number of

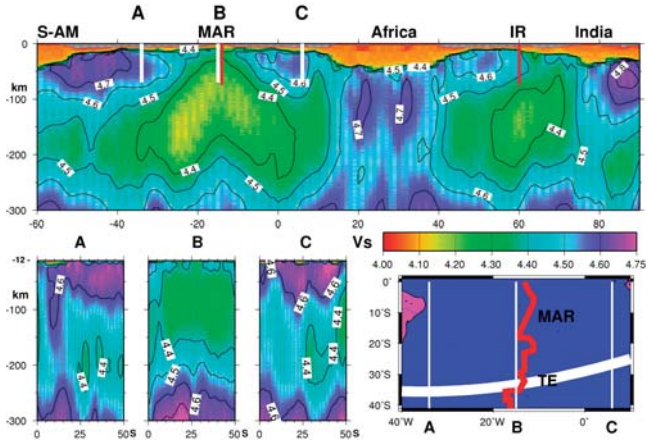

Figure 3. Above, enlarged shear wave velocity (Vs) cross section of Mid-Atlantic Ridge (MAR) and Indian Ridge (IR) along tectonic equator (TE). S-AM—South America. Unlike Figure 1, velocities are unsmoothed. Below, A–C are north-south cross sections parallel to southern MAR (see small map with MAR in red). S-AM—South America. Western side of ridge shows faster lithosphere and slower asthenosphere, both moving perpendicular and parallel to ridge. Data from CUB2 model (see text).

parameters, such as the tectonic setting (e.g., smaller along transtensive rifts), the original mantle composition and fluids contents, and the temperature of the mantle. The variation in Vs is by definition associated with the variation of the square root of the ratio between rigidity (μ) and density (ρ). However, it remains unknown, at least to our knowledge, how to relate in detail the variation of those parameters with the mantle modification at ridges. Oxburgh and Parmentier (1977) suggested that there is mantle depletion along ridges, regardless of whether the rift is symmetric or asymmetric. From tomography images (see Pilidou et al., 2005), all we can say is that the ratio μ/ρ is different between the two sides of the ridges. Moreover, the mean bathymetry is slightly shallower in the eastern flank of the rifts. Therefore, due to the westerly migration of ridges and of the lithosphere relative to the underlying mantle, we interpret the asymmetry as the result of an oblique upraising of the mantle and the distribution of the related depletion.

RADIAL ANISOTROPY

Detailed information on the seismic anisotropy of the Earth's mantle provides insight into paleodeformation and recent deformation processes and therefore mantle dynamics. Radial anisotropy of shear velocities in the upper mantle is usually characterized by the ratio $\eta = (Vsh - Vsv)/Vs$ (in percent), where Vsh and Vsv are velocities of two types of shear waves of different polarization and $Vs = (Vsh + Vsv)/2$.

In the anisotropy sections, both along the TE and TE-pert, the minimum value of radial anisotropy is reached, in general at a depth of ~200 km, with outstanding exceptions in proximity of the ridges. The level at which radial anisotropy is low, e.g., <1%, may represent the decoupling level between the lithosphere and the underlying asthenospheric low-velocity layer, due to the presence of a relevant fraction of melt that inhibits the formation of preferential orientations in the texture of mantle rocks. In particular, along the TE-pert, very low values of radial anisotropy (<1%) reach the top of the section (20 km below surface) with an eastward shift of ~20° with respect to the East Pacific Ridge and Mid-Atlantic Ridge, and a smaller shift is seen along TE, with respect to the East Pacific Ridge, all in agreement with the notion of westward drift of the lithosphere relative to the underlying mantle (first-order flow). From Figure 1, it can be inferred that the shift between the geographical ridges axis and the vertical stripes of radial anisotropy <1% (the anisotropy ridge) axis varies from ~1250 to 2500 km (eastward). The formation of a sizeable solid lid at the ridge sides requires no more than 10–20 m.y. (e.g., Leeds et al., 1974; Forsyth, 1975; Panza, 1980), and both a systematic increase in velocities with the age of the seafloor and anisotropy of propagation are observed (Forsyth, 1975). From the above values one gets an average westward lithosphere velocity of ~12.5 cm/yr. This value is the result of the ratio between the extremes of the space and time intervals.

The exception of the Mid-Atlantic Ridge along the TE section is only apparent; in fact, the relatively high radial anisotropy there can be explained by the fact that the TE intersects the Mid-Atlantic Ridge where the ridge makes an almost 90° bend, thus giving rise to apparent anisotropy related to geometry rather than rock texture.

DISCUSSION AND CONCLUSIONS

We show relevant horizontal Vs variations both in the lithosphere (uppermost ~100 km of the Earth) and in the upper asthenosphere (low-velocity layer, from ~100–200 km of depth). However, the low-velocity layer in the upper asthenosphere is recognized all across the Earth as a persistent layer at the depth of 120–200 km, as shown in a modified path of the TE. Across rift zones the main velocity variation is ~0.1–0.3 km/s, where the western flank has a faster lithosphere and a slower asthenosphere relative to the eastern or northeastern flank. Whatever the cause, rift zones show a worldwide mean signature in terms of asymmetry, with a stronger Vs contrast between lithosphere and asthenosphere in the western limb when compared to the eastern one. We interpret it as the depletion of the asthenosphere along the rift, while the ridge is moving westward relative to the mantle. The lithosphere to the east would represent the cooling of the more depleted asthenosphere, abandoned after the ridge migration to the west. This process is consistent with the net rotation of the lithosphere relative to the underlying mantle. This decoupling is postulated by the sizeable amount of melting that can be inferred from Vs and radial anisotropy sections at ~190–220 km (Fig. 1). In this interpretation, beneath the decoupling, the mantle shifts eastward relative to the lithosphere (first-order flow). This relative motion could be responsible for the main anisotropy recorded by shear wave splitting analysis (e.g., Debayle et al., 2005). Along ridges, the oblique rising mantle could be responsible for the asymmetric pattern (second-order flow, Fig. 4). The heterogeneity among the flanks of ocean basins mirrors the differences of subduction zones as a function of their geographic polarity. This polarization along the TE points to an asymmetric Earth, as expected for a complete net rotation of the lithosphere (1.20°/m.y.; Crespi et al., 2007).

ACKNOWLEDGMENTS

Discussions with E. Carminati, M. Cuffaro, D. Forsyth, F. Innocenti, and F. Riguzzi were very helpful. The article benefited by the critical reviews of Enrico Bonatti, L. Husson, and two anonymous referees, and constructive criticisms by the editor S.J. Wyld. We appreciate the opportunity to have access to the tomographic model CUB2 by Nikolai Shapiro and Michael Ritzwoller. Parts of figures have been plotted using GMT (Generic Mapping Tools; Wessel and Smith, 1995). M. Cuffaro provided technical support. Research was supported by Eurocores-CNR (TopoEurope-Topo4D project).

REFERENCES CITED

Bonatti, E., Gasperini, L., Brunelli, D., Ligi, M., Ottolini, L., Ferrante, V., Cipriani, A., and Fabretti, P., 2003, Mantle thermal pulses below the Mid-Atlantic Ridge and temporal variations in the formation of oceanic lithosphere: Nature, v. 423, p. 499–505, doi: 10.1038/nature01594.

Calcagno, P., and Cazenave, A., 1994, Subsidence of the seafloor in the Atlantic and Pacific oceans; regional and large-scale variations: Earth and Planetary Science Letters, v. 126, p. 473–492, doi: 10.1016/0012-821X(94)90125-2.

Cande, S.C., and Kent, D.V., 1995, Revised calibration of the geomagnetic polarity time scale for the

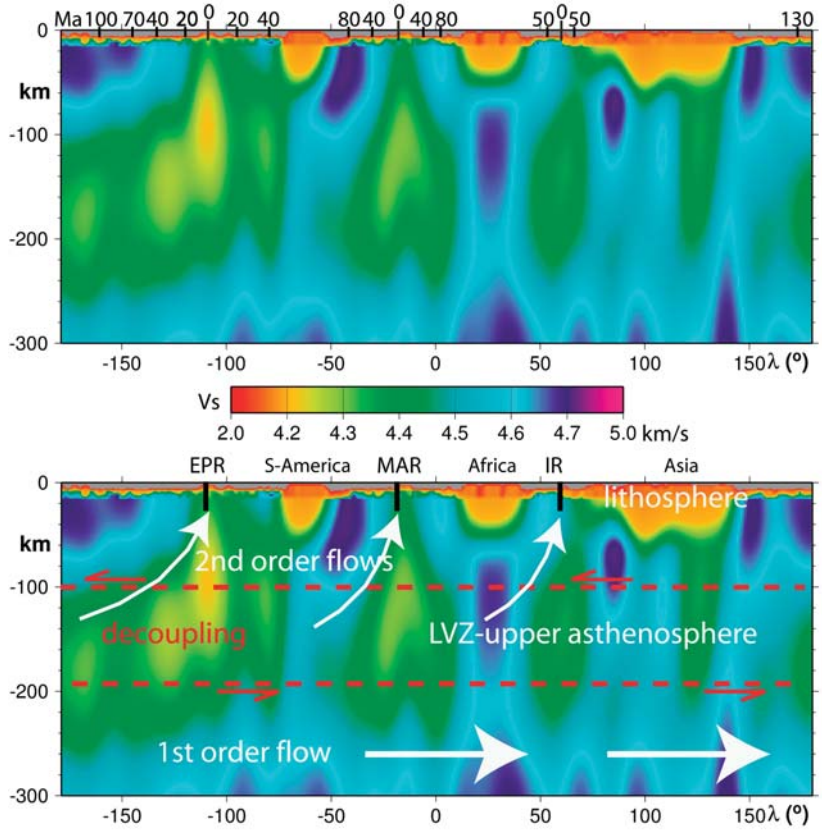

Figure 4. Uninterpreted (above) and interpreted (below) shear wave velocity (Vs) sections along tectonic equator of Earth's first 300 km. EPR—Eastern Pacific Ridge, MAR—Mid-Atlantic Ridge, IR—Indian Ridge. Upper asthenosphere contains low-velocity layer (LVZ), i.e., what is supposed to be main decoupling surface between lithosphere and mantle, allowing net rotation of lithosphere, i.e., first-order relative eastward relative mantle flow, or westward drift of lithosphere. Secondary flow should be related to mantle obliquely upraised along oceanic ridges. Asymmetry between two sides of ridges is independent from age of oceanic lithosphere, shown at top in million years (Ma; ages from Müller et al., 2008).

Late Cretaceous and Cenozoic: Journal of Geophysical Research, v. 100, no. B4, p. 6093–6095.

Cann, J.R., Elderfield, H., and Laughton, A.S., eds., 1999, Mid-ocean ridges, dynamics of processes associated with the creation of new oceanic crust: Cambridge, Cambridge University Press, 301 p.

Crespi, M., Cuffaro, M., Doglioni, C., Giannone, F., and Riguzzi, F., 2007, Space geodesy validation of the global lithospheric flow: Geophysical Journal International, v. 168, p. 491–506, doi: 10.1111/j.1365-246X.2006.03226.x.

Debayle, E., Kennett, B., and Priestley, K., 2005, Global azimuthal seismic anisotropy and the unique plate-motion deformation of Australia: Nature, v. 433, p. 509–512, doi: 10.1038/nature03247.

Doglioni, C., Carminati, E., and Bonatti, E., 2003, Rift asymmetry and continental uplift: Tectonics, v. 22, 1024, doi: 10.1029/2002TC001459.

Doglioni, C., Green, D., and Mongelli, F., 2005, On the shallow origin of hotspots and the westward drift of the lithosphere, *in* Foulger, G.R., et al., eds., Plates, plumes and paradigms: Geological Society of America Special Paper 388, p. 735–749, doi: 10.1130/0-8137-2388-4.735.

Doglioni, C., Carminati, E., Cuffaro, M., and Scrocca, D., 2007, Subduction kinematics and dynamic constraints: Earth-Science Reviews, v. 83, p. 125–175, doi: 10.1016/j.earscirev.2007.04.001.

Ekstrom, G., Tromp, J., and Larson, E.W.F., 1997, Measurements and global models of surface wave propagation: Journal of Geophysical Research, v. 102, p. 8137–8157, doi: 10.1029/96JB03729.

Forsyth, D.W., 1975, The early structural evolution and anisotropy of the oceanic upper mantle: Royal Astronomical Society Geophysical Journal, v. 43, p. 103–162, doi: 10.1111/j.1365-246X.1975.tb00630.x.

Garfunkel, Z., Anderson, C.A., and Schubert, G., 1986, Mantle circulation and the lateral migration of subducted slabs: Journal of Geophysical Research, v. 91, no. B7, p. 7205–7223, doi: 10.1029/JB091iB07p07205.

Gripp, A.E., and Gordon, R.G., 2002, Young tracks of hotspots and current plate velocities: Geophysical Journal International, v. 150, p. 321–361, doi: 10.1046/j.1365-246X.2002.01627.x.

Husson, L., Conrad, C.P., and Faccenna, C., 2008, Tethyan closure, Andean orogeny, and westward drift of the Pacific Basin: Earth and Planetary Science Letters, v. 271, p. 303–310, doi: 10.1016/j.epsl.2008.04.022.

Leeds, A.R., Knopoff, L., and Kausel, E., 1974, Variations of upper mantle structure under the Pacific Ocean: Science, v. 186, p. 141–143, doi: 10.1126/science.186.4159.141.

Le Pichon, X., 1968, Sea-floor spreading and continental drift: Journal of Geophysical Research, v. 73, no. 12, p. 3661–3697, doi: 10.1029/JB073i012p03661.

Levshin, A.L., Yanovskaya, T.B., Lander, A.V., Bukchin, B.G., Barmin, M.P., Ratnikova, L.I., and Its, E.N., 1989, Seismic surface waves in laterally inhomogeneous Earth: Modern approaches to geophysics, Volume 9: Dordrecht, Netherlands, Kluwer, 304 p.

Morgan, J.P., and Smith, W.H.E., 1992, Flattening of the sea-floor depth-age curve as a response to asthenospheric flow: Nature, v. 359, p. 524–527, doi: 10.1038/359524a0.

Müller, R.D., Sdrolias, M., Gaina, C., and Roest, W.R., 2008, Age, spreading rates and spreading asymmetry of the world's ocean crust: Geochemistry Geophysics Geosystems, v. 9, Q04006, doi: 10.1029/2007GC001743.

Oxburgh, E.R., and Parmentier, E.M., 1977, Compositional and density stratification in oceanic lithosphere; causes and consequences: Geological Society of London Journal, v. 133, p. 343–355, doi: 10.1144/gsjgs.133.4.0343.

Panza, G.F., 1980, Evolution of the Earth's lithosphere, *in* Davies, P.A., and Runcorn, S.K., eds., Mechanisms of continental drift and plate tectonics: London, Academic Press, p. 75–87.

Pilidou, S., Priestley, K., Debayle, E., and Gudmundsson, O., 2005, Rayleigh wave tomography in the North Atlantic: High resolution images of the Iceland, Azores and Eifel mantle plumes: Lithos, v. 79, p. 453–474, doi: 10.1016/j.lithos.2004.09.012.

Ritzwoller, M.H., and Levshin, A.L., 1998, Eurasian surface wave tomography: Group velocities: Journal of Geophysical Research, v. 103, p. 4839–4878, doi: 10.1029/97JB02622.

Ritzwoller, M.H., Shapiro, N.M., Barmin, M.P., and Levshin, A., 2002, Global surface wave diffraction tomography: Journal of Geophysical Research, v. 107, no. B12, p. 2335–2348, doi: 10.1029/2002JB001777.

Scheirer, D.S., Forsyth, D.W., Cormier, M.H., and Macdonald, K.C., 1998, Shipboard geophysical indications of asymmetry and melt production beneath the East Pacific Rise near the MELT experiment: Science, v. 280, p. 1221–1224, doi: 10.1126/science.280.5367.1221.

Scoppola, B., Boccaletti, D., Bevis, M., Carminati, E., and Doglioni, C., 2006, The westward drift of the lithosphere: A rotational drag?: Geological Society of America Bulletin, v. 118, p. 199–209, doi: 10.1130/B25734.1.

Shapiro, N.M., and Ritzwoller, M.H., 2002, Monte-Carlo inversion for a global shear velocity model of the crust and upper mantle: Geophysical Journal International, v. 151, p. 88–105, doi: 10.1046/j.1365-246X.2002.01742.x.

Trampert, J., and Woodhouse, J.H., 1995, Global phase velocity maps of Love and Rayleigh waves between 40 and 150 s: Geophysical Journal International, v. 122, p. 675–690, doi: 10.1111/j.1365-246X.1995.tb07019.x.

Wessel, P.A., and Smith, W.H., 1995, New version of the Generic Mapping Tools released: Eos (Transactions, American Geophysical Union), v. 76, supplement, p. 329, doi: 10.1029/95EO00198.

Zhang, Y.S., and Tanimoto, T., 1993, High-resolution global upper mantle structure and plate tectonics: Journal of Geophysical Research, v. 98, no. B6, p. 9793–9823, doi: 10.1029/93JB00148.

Manuscript received 28 July 2009
Revised manuscript received 5 August 2009
Manuscript accepted 10 August 2009

Printed in USA

Figure DR1. Bathymetry

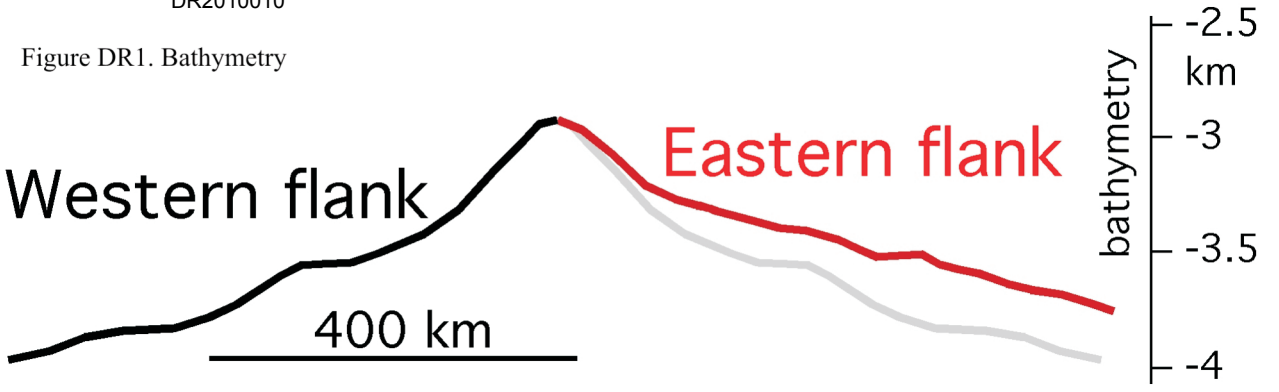

Figure DR2. Pacific section.

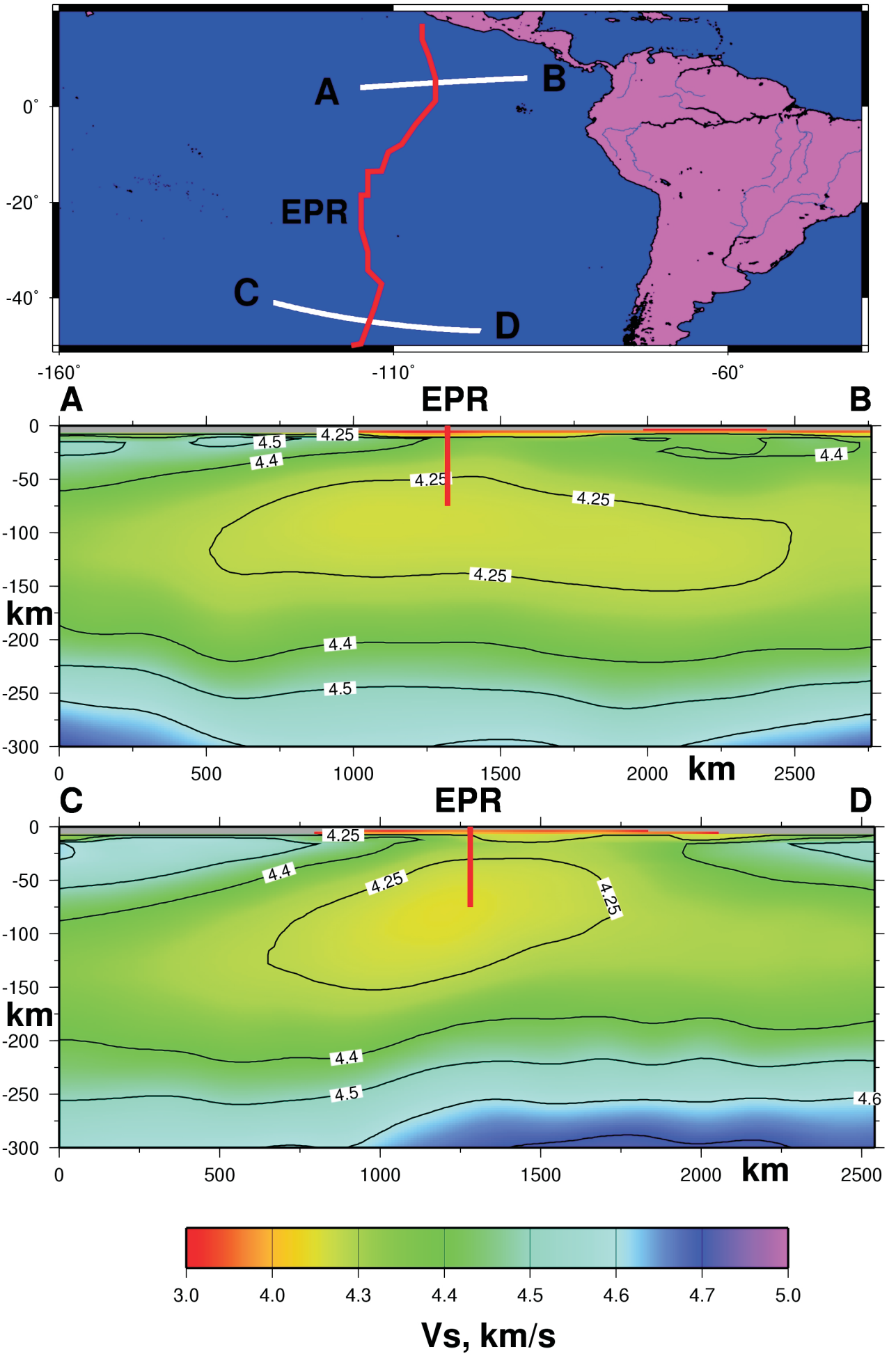

Figure DR3. Atlantic section.

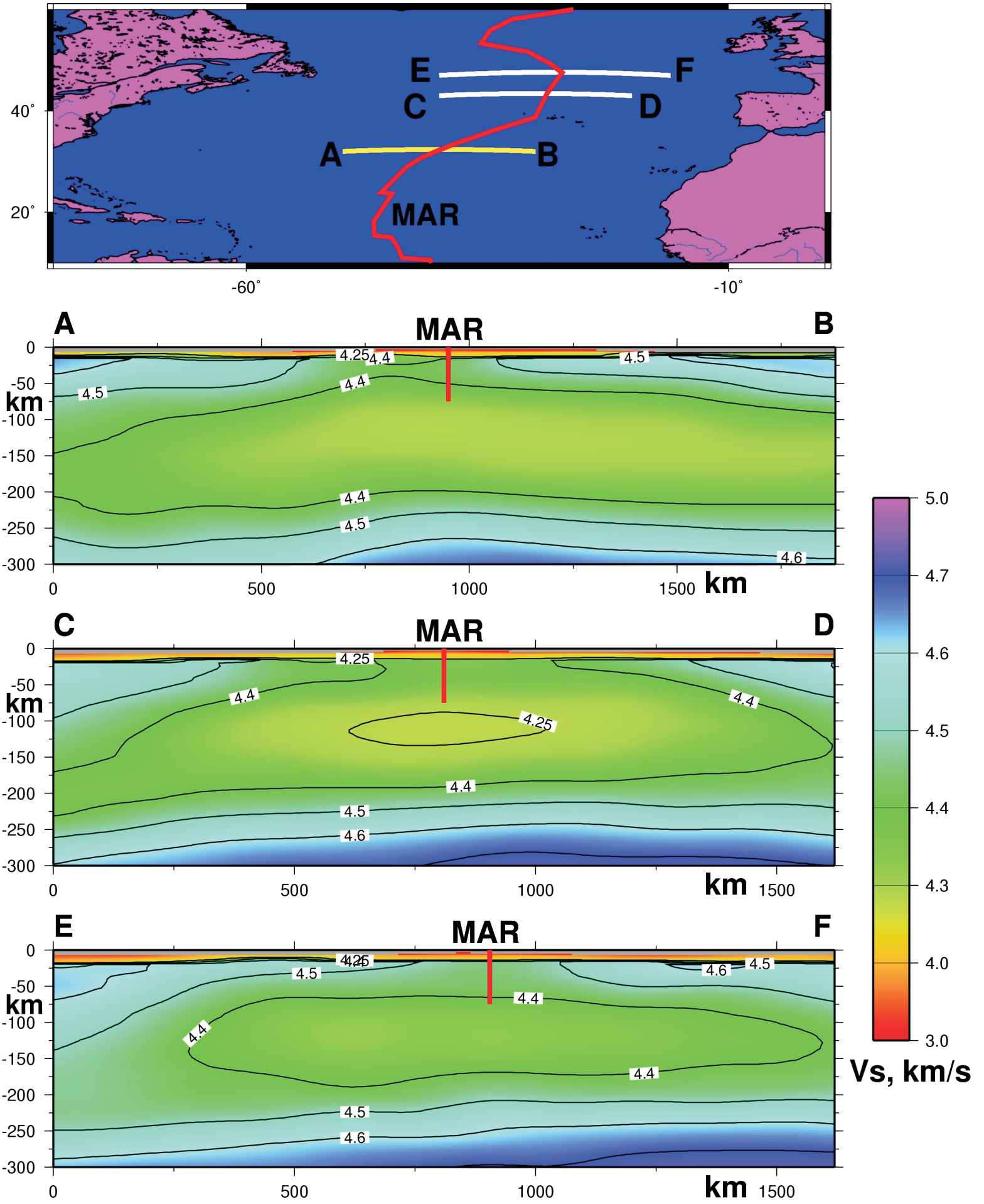

Figure DR4. Indian Ocean section.

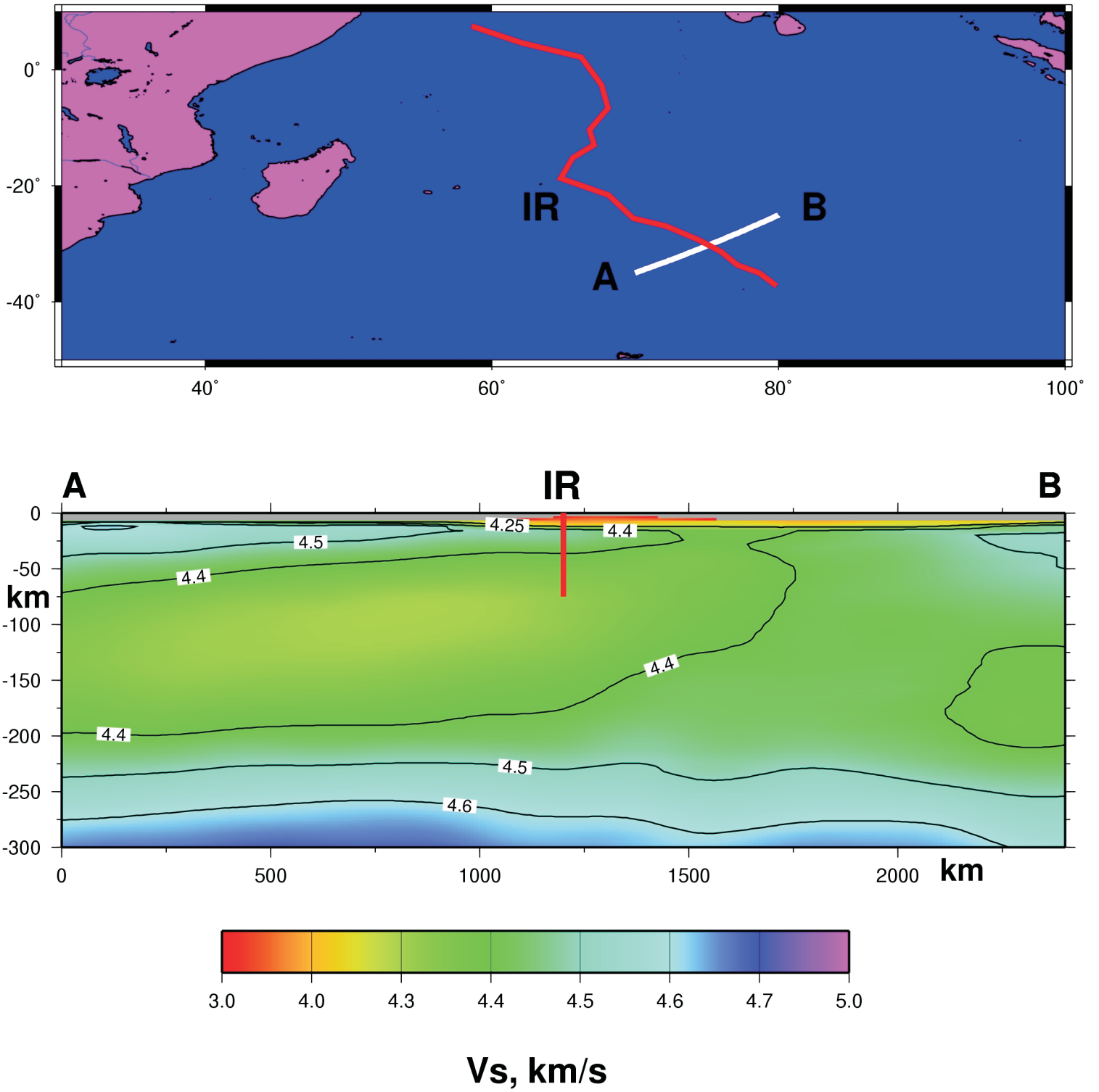

Table DR1. Geographic coordinates,TE_TE_pert

Coordinates of the tectonic equator (TE)

-179.0000	28.6270
-178.0000	28.2540
-177.0000	27.8720
-176.0000	27.4820
-175.0000	27.0840
-174.0000	26.6770
-173.0000	26.2620
-172.0000	25.8390
-171.0000	25.4080
-170.0000	24.9700
-169.0000	24.5230
-168.0000	24.0700
-167.0000	23.6090
-166.0000	23.1410
-165.0000	22.6650
-164.0000	22.1830
-163.0000	21.6940
-162.0000	21.1990
-161.0000	20.6970
-160.0000	20.1890
-159.0000	19.6740
-158.0000	19.1540
-157.0000	18.6280
-156.0000	18.0960
-155.0000	17.5580
-154.0000	17.0160
-153.0000	16.4680
-152.0000	15.9150
-151.0000	15.3570
-150.0000	14.7940
-149.0000	14.2270
-148.0000	13.6560
-147.0000	13.0810
-146.0000	12.5010
-145.0000	11.9180
-144.0000	11.3310
-143.0000	10.7410

-142.0000	10.1470
-141.0000	9.5500
-140.0000	8.9510
-139.0000	8.3480
-138.0000	7.7430
-137.0000	7.1360
-136.0000	6.5270
-135.0000	5.9150
-134.0000	5.3020
-133.0000	4.6870
-132.0000	4.0710
-131.0000	3.4530
-130.0000	2.8350
-129.0000	2.2150
-128.0000	1.5950
-127.0000	0.9750
-126.0000	0.3540
-125.0000	-0.2670
-124.0000	-0.8880
-123.0000	-1.5090
-122.0000	-2.1290
-121.0000	-2.7480
-120.0000	-3.3670
-119.0000	-3.9850
-118.0000	-4.6010
-117.0000	-5.2160
-116.0000	-5.8300
-115.0000	-6.4410
-114.0000	-7.0510
-113.0000	-7.6590
-112.0000	-8.2640
-111.0000	-8.8670
-110.0000	-9.4670
-109.0000	-10.0640
-108.0000	-10.6580
-107.0000	-11.2490
-106.0000	-11.8360
-105.0000	-12.4200
-104.0000	-13.0000
-103.0000	-13.5760
-102.0000	-14.1480
-101.0000	-14.7160
-100.0000	-15.2790

-99.0000	-15.8370
-98.0000	-16.3910
-97.0000	-16.9390
-96.0000	-17.4830
-95.0000	-18.0210
-94.0000	-18.5540
-93.0000	-19.0810
-92.0000	-19.6020
-91.0000	-20.1170
-90.0000	-20.6260
-89.0000	-21.1290
-88.0000	-21.6260
-87.0000	-22.1150
-86.0000	-22.5990
-85.0000	-23.0750
-84.0000	-23.5440
-83.0000	-24.0060
-82.0000	-24.4610
-81.0000	-24.9080
-80.0000	-25.3470
-79.0000	-25.7790
-78.0000	-26.2030
-77.0000	-26.6190
-76.0000	-27.0270
-75.0000	-27.4270
-74.0000	-27.8190
-73.0000	-28.2010
-72.0000	-28.5760
-71.0000	-28.9410
-70.0000	-29.2980
-69.0000	-29.6460
-68.0000	-29.9850
-67.0000	-30.3150
-66.0000	-30.6350
-65.0000	-30.9460
-64.0000	-31.2480
-63.0000	-31.5400
-62.0000	-31.8230
-61.0000	-32.0960
-60.0000	-32.3590
-59.0000	-32.6120
-58.0000	-32.8550
-57.0000	-33.0890

-56.0000	-33.3120
-55.0000	-33.5250
-54.0000	-33.7280
-53.0000	-33.9210
-52.0000	-34.1030
-51.0000	-34.2750
-50.0000	-34.4360
-49.0000	-34.5870
-48.0000	-34.7280
-47.0000	-34.8580
-46.0000	-34.9770
-45.0000	-35.0850
-44.0000	-35.1830
-43.0000	-35.2700
-42.0000	-35.3470
-41.0000	-35.4120
-40.0000	-35.4670
-39.0000	-35.5110
-38.0000	-35.5450
-37.0000	-35.5670
-36.0000	-35.5790
-35.0000	-35.5790
-34.0000	-35.5690
-33.0000	-35.5480
-32.0000	-35.5170
-31.0000	-35.4740
-30.0000	-35.4210
-29.0000	-35.3570
-28.0000	-35.2820
-27.0000	-35.1960
-26.0000	-35.1000
-25.0000	-34.9930
-24.0000	-34.8750
-23.0000	-34.7460
-22.0000	-34.6070
-21.0000	-34.4580
-20.0000	-34.2980
-19.0000	-34.1280
-18.0000	-33.9470
-17.0000	-33.7560
-16.0000	-33.5540
-15.0000	-33.3420
-14.0000	-33.1210

-13.0000	-32.8890
-12.0000	-32.6470
-11.0000	-32.3950
-10.0000	-32.1330
-9.0000	-31.8620
-8.0000	-31.5800
-7.0000	-31.2890
-6.0000	-30.9890
-5.0000	-30.6790
-4.0000	-30.3600
-3.0000	-30.0320
-2.0000	-29.6940
-1.0000	-29.3470
0.0000	-28.9920
1.0000	-28.6270
2.0000	-28.2540
3.0000	-27.8720
4.0000	-27.4820
5.0000	-27.0840
6.0000	-26.6770
7.0000	-26.2620
8.0000	-25.8390
9.0000	-25.4080
10.0000	-24.9690
11.0000	-24.5230
12.0000	-24.0700
13.0000	-23.6090
14.0000	-23.1410
15.0000	-22.6650
16.0000	-22.1830
17.0000	-21.6940
18.0000	-21.1990
19.0000	-20.6970
20.0000	-20.1890
21.0000	-19.6740
22.0000	-19.1540
23.0000	-18.6280
24.0000	-18.0960
25.0000	-17.5580
26.0000	-17.0160
27.0000	-16.4680
28.0000	-15.9150
29.0000	-15.3570

30.0000	-14.7940
31.0000	-14.2270
32.0000	-13.6560
33.0000	-13.0800
34.0000	-12.5010
35.0000	-11.9180
36.0000	-11.3310
37.0000	-10.7400
38.0000	-10.1470
39.0000	-9.5500
40.0000	-8.9500
41.0000	-8.3480
42.0000	-7.7430
43.0000	-7.1360
44.0000	-6.5270
45.0000	-5.9150
46.0000	-5.3020
47.0000	-4.6870
48.0000	-4.0710
49.0000	-3.4530
50.0000	-2.8350
51.0000	-2.2150
52.0000	-1.5950
53.0000	-0.9750
54.0000	-0.3540
55.0000	0.2670
56.0000	0.8880
57.0000	1.5090
58.0000	2.1290
59.0000	2.7490
60.0000	3.3670
61.0000	3.9850
62.0000	4.6010
63.0000	5.2160
64.0000	5.8300
65.0000	6.4420
66.0000	7.0510
67.0000	7.6590
68.0000	8.2640
69.0000	8.8670
70.0000	9.4670
71.0000	10.0640
72.0000	10.6580

73.0000	11.2490
74.0000	11.8360
75.0000	12.4200
76.0000	13.0000
77.0000	13.5760
78.0000	14.1480
79.0000	14.7160
80.0000	15.2790
81.0000	15.8370
82.0000	16.3910
83.0000	16.9400
84.0000	17.4830
85.0000	18.0210
86.0000	18.5540
87.0000	19.0810
88.0000	19.6020
89.0000	20.1170
90.0000	20.6260
91.0000	21.1290
92.0000	21.6260
93.0000	22.1160
94.0000	22.5990
95.0000	23.0750
96.0000	23.5440
97.0000	24.0060
98.0000	24.4610
99.0000	24.9080
100.0000	25.3470
101.0000	25.7790
102.0000	26.2030
103.0000	26.6200
104.0000	27.0270
105.0000	27.4270
106.0000	27.8190
107.0000	28.2020
108.0000	28.5760
109.0000	28.9410
110.0000	29.2980
111.0000	29.6460
112.0000	29.9850
113.0000	30.3150
114.0000	30.6350
115.0000	30.9460

116.0000	31.2480
117.0000	31.5400
118.0000	31.8230
119.0000	32.0960
120.0000	32.3590
121.0000	32.6120
122.0000	32.8550
123.0000	33.0890
124.0000	33.3120
125.0000	33.5250
126.0000	33.7280
127.0000	33.9210
128.0000	34.1030
129.0000	34.2750
130.0000	34.4360
131.0000	34.5870
132.0000	34.7280
133.0000	34.8580
134.0000	34.9770
135.0000	35.0850
136.0000	35.1830
137.0000	35.2700
138.0000	35.3470
139.0000	35.4120
140.0000	35.4670
141.0000	35.5110
142.0000	35.5450
143.0000	35.5670
144.0000	35.5790
145.0000	35.5790
146.0000	35.5690
147.0000	35.5480
148.0000	35.5170
149.0000	35.4740
150.0000	35.4210
151.0000	35.3570
152.0000	35.2820
153.0000	35.1960
154.0000	35.1000
155.0000	34.9930
156.0000	34.8750
157.0000	34.7460
158.0000	34.6070

159.0000	34.4580
160.0000	34.2980
161.0000	34.1280
162.0000	33.9470
163.0000	33.7560
164.0000	33.5540
165.0000	33.3420
166.0000	33.1210
167.0000	32.8890
168.0000	32.6470
169.0000	32.3950
170.0000	32.1330
171.0000	31.8610
172.0000	31.5800
173.0000	31.2890
174.0000	30.9890
175.0000	30.6790
176.0000	30.3600
177.0000	30.0320
178.0000	29.6940
179.0000	29.3470
180.0000	28.9920

Coordinates of the tectonic equator perturbed (TE_Perturbed)

-179.0000	28.6270
-178.0000	28.2540
-177.0000	27.8720
-176.0000	27.4820
-175.0000	27.0840
-174.0000	26.6770
-173.0000	26.2620
-172.0000	25.8390
-171.0000	25.4080
-170.0000	24.9700
-169.0000	24.5230
-168.0000	24.0700
-167.0000	23.6090
-166.0000	23.1410
-165.0000	22.6650
-164.0000	22.1830
-163.0000	21.6940

-162.0000	21.1990
-161.0000	20.6970
-160.0000	20.1890
-159.0000	19.6740
-158.0000	19.1540
-157.0000	18.6280
-156.0000	18.0960
-155.0000	17.5580
-154.0000	17.0160
-153.0000	16.4680
-152.0000	15.9150
-151.0000	15.3570
-150.0000	14.7940
-149.0000	14.2270
-148.0000	13.6560
-147.0000	13.0810
-146.0000	12.5010
-145.0000	11.9180
-144.0000	11.3310
-143.0000	10.7410
-142.0000	10.1470
-141.0000	9.5500
-140.0000	8.9510
-139.0000	8.3480
-138.0000	7.7430
-137.0000	7.1360
-136.0000	6.5270
-135.0000	5.9150
-134.0000	5.3020
-133.0000	4.6870
-132.0000	4.0710
-131.0000	3.4530
-130.0000	2.8350
-129.0000	2.2150
-128.0000	1.5950
-127.0000	0.9750
-126.0000	0.3540
-125.0000	-0.2867
-124.0000	-0.9669
-123.0000	-1.6861
-122.0000	-2.4432
-121.0000	-3.2374
-120.0000	-4.0692

-119.0000	-4.9367
-118.0000	-5.8379
-117.0000	-6.7727
-116.0000	-7.7398
-115.0000	-8.7359
-114.0000	-9.7613
-113.0000	-10.8135
-112.0000	-11.8898
-111.0000	-12.9891
-110.0000	-14.1087
-109.0000	-15.2465
-108.0000	-16.4002
-107.0000	-17.5677
-106.0000	-18.7458
-105.0000	-19.9331
-104.0000	-21.1262
-103.0000	-22.3227
-102.0000	-23.5201
-101.0000	-24.7160
-100.0000	-25.9069
-99.0000	-27.0903
-98.0000	-28.2648
-97.0000	-29.4259
-96.0000	-30.5732
-95.0000	-31.7022
-94.0000	-32.8118
-93.0000	-33.8985
-92.0000	-34.9603
-91.0000	-35.9948
-90.0000	-37.0002
-89.0000	-37.9745
-88.0000	-38.9157
-87.0000	-39.8201
-86.0000	-40.6892
-85.0000	-41.5183
-84.0000	-42.3071
-83.0000	-43.0543
-82.0000	-43.7588
-81.0000	-44.4186
-80.0000	-45.0328
-79.0000	-45.6019
-78.0000	-46.1241
-77.0000	-46.5993

-76.0000	-47.0270
-75.0000	-47.4270
-74.0000	-47.8190
-73.0000	-48.2010
-72.0000	-48.5760
-71.0000	-48.9410
-70.0000	-49.2980
-69.0000	-49.6460
-68.0000	-49.9850
-67.0000	-50.3150
-66.0000	-50.6350
-65.0000	-50.9460
-64.0000	-51.2480
-63.0000	-51.5400
-62.0000	-51.8230
-61.0000	-52.0960
-60.0000	-52.3590
-59.0000	-52.6120
-58.0000	-52.8550
-57.0000	-53.0890
-56.0000	-53.3120
-55.0000	-53.5250
-54.0000	-53.7280
-53.0000	-53.9210
-52.0000	-54.1030
-51.0000	-54.2750
-50.0000	-54.4360
-49.0000	-54.5870
-48.0000	-54.7280
-47.0000	-54.8580
-46.0000	-54.9770
-45.0000	-55.0850
-44.0000	-55.1830
-43.0000	-55.2700
-42.0000	-55.3470
-41.0000	-55.4120
-40.0000	-55.4670
-39.0000	-55.5110
-38.0000	-55.5450
-37.0000	-55.5670
-36.0000	-55.5790
-35.0000	-55.5790
-34.0000	-55.5690

-33.0000	-55.5480
-32.0000	-55.5170
-31.0000	-55.4740
-30.0000	-55.4210
-29.0000	-55.3570
-28.0000	-55.2820
-27.0000	-55.1960
-26.0000	-55.1000
-25.0000	-54.9930
-24.0000	-54.8750
-23.0000	-54.7460
-22.0000	-54.6070
-21.0000	-54.4580
-20.0000	-54.2980
-19.0000	-54.1280
-18.0000	-53.9470
-17.0000	-53.7560
-16.0000	-53.5540
-15.0000	-53.3420
-14.0000	-53.1210
-13.0000	-52.8890
-12.0000	-52.6470
-11.0000	-52.3950
-10.0000	-52.1330
-9.0000	-51.8620
-8.0000	-51.5800
-7.0000	-51.2890
-6.0000	-50.9890
-5.0000	-50.6790
-4.0000	-50.3600
-3.0000	-50.0320
-2.0000	-49.6940
-1.0000	-49.3470
0.0000	-48.9920
1.0000	-48.6270
2.0000	-48.2540
3.0000	-47.8720
4.0000	-47.4820
5.0000	-47.0840
6.0000	-46.6770
7.0000	-46.2620
8.0000	-45.8390
9.0000	-45.4080

10.0000	-44.9690
11.0000	-44.5230
12.0000	-44.0700
13.0000	-43.6090
14.0000	-43.1410
15.0000	-42.6650
16.0000	-42.1830
17.0000	-41.6940
18.0000	-41.1990
19.0000	-40.6970
20.0000	-40.1890
21.0000	-39.6740
22.0000	-39.1540
23.0000	-38.6280
24.0000	-38.0960
25.0000	-37.5580
26.0000	-37.0160
27.0000	-36.4680
28.0000	-35.9150
29.0000	-35.3570
30.0000	-34.7940
31.0000	-34.2270
32.0000	-33.6560
33.0000	-33.0800
34.0000	-32.5010
35.0000	-31.9180
36.0000	-31.3310
37.0000	-30.7400
38.0000	-30.1470
39.0000	-29.5500
40.0000	-28.9500
41.0000	-28.3480
42.0000	-27.7430
43.0000	-27.1360
44.0000	-26.5270
45.0000	-25.9150
46.0000	-25.3020
47.0000	-24.6870
48.0000	-24.0710
49.0000	-23.4530
50.0000	-22.8350
51.0000	-22.2150
52.0000	-21.5950

53.0000	-20.9750
54.0000	-20.3540
55.0000	-19.7330
56.0000	-19.1120
57.0000	-18.4910
58.0000	-17.8710
59.0000	-17.2510
60.0000	-16.6330
61.0000	-16.0150
62.0000	-15.3990
63.0000	-14.7840
64.0000	-14.1700
65.0000	-13.5580
66.0000	-12.9490
67.0000	-12.3410
68.0000	-11.7360
69.0000	-11.1330
70.0000	-10.5330
71.0000	-9.9360
72.0000	-9.3420
73.0000	-8.7510
74.0000	-8.1640
75.0000	-7.5800
76.0000	-7.0000
77.0000	-6.4240
78.0000	-5.8520
79.0000	-5.2840
80.0000	-4.72100
81.0000	-4.25932
82.0000	-3.79763
83.0000	-3.33595
84.0000	-2.87426
85.0000	-2.41258
86.0000	-1.95089
87.0000	-1.48920
88.0000	-1.02752
89.0000	-0.565835
90.0000	-1.04150E-01
91.0000	0.357535
92.0000	0.819220
93.0000	1.28091
94.0000	1.74259
95.0000	2.20428

96.0000	2.66596
97.0000	3.12765
98.0000	3.58933
99.0000	4.05102
100.0000	4.51270
101.0000	4.97439
102.0000	5.43607
103.0000	5.89776
104.0000	6.35944
105.0000	6.82113
106.000	7.28281
107.000	7.74450
108.000	8.20618
109.000	8.66787
110.000	9.12955
111.000	9.59124
112.000	10.05292
113.000	10.51461
114.000	10.9763
115.000	11.4380
116.000	11.8997
117.000	12.3613
118.000	12.8230
119.000	13.2847
120.000	13.7464
121.000	14.2081
122.000	14.6698
123.000	15.1315
124.000	15.5931
125.000	16.0548
126.000	16.5165
127.000	16.9782
128.000	17.4399
129.000	17.9016
130.000	18.3633
131.000	18.8249
132.000	19.2866
133.000	19.7483
134.000	20.2100
135.000	20.6717
136.000	21.1334
137.000	21.5950
138.000	22.0567

139.000	22.5184
140.000	22.9801
161.0000	32.8911
162.0000	32.9953
163.0000	33.0538
164.0000	33.0646
165.0000	33.0278
166.0000	32.9439
167.0000	32.8101
168.0000	32.6273
169.0000	32.3950
170.0000	32.1330
171.0000	31.8610
172.0000	31.5800
173.0000	31.2890
174.0000	30.9890
175.0000	30.6790
176.0000	30.3600
177.0000	30.0320
178.0000	29.6940
179.0000	29.3470
180.0000	28.9920